Batteries & Supercaps

Research Article
doi.org/10.1002/batt.202300352

Chemistry
Europe
European Chemical
Societies Publishing

www.batteries-supercaps.org

Deciphering the Nature of an Overlooked Rate-Limiting Interphase in High-Voltage LiNi$_{0.5}$Mn$_{1.5}$O$_4$ Cathodes: A Combined Electrochemical Impedance, Scanning Electron Microscopy and Secondary Ion Mass Spectrometry Study

Lars Pateras Pescara,[a] Andrea Jaegermann,[a] Valeriu Mereacre,[b] Marvin Cronau,[a] Joachim R. Binder,[b] and Bernhard Roling*[a]

High-voltage cathode active materials, such as LiNi$_{0.5}$Mn$_{1.5}$O$_4$ (LNMO), are of major interest for the development of high-energy lithium-ion batteries. However, it has been reported that composite cathodes based on high-voltage active materials suffer from high impedances and low rate capabilities. The origin of the high impedances has not yet been clarified. Here, we use a combination of electrochemical impedance spectroscopy (EIS), focused ion beam/scanning electron microscopy/energy-dispersive X-ray spectroscopy (FIB/SEM/EDX) and time-of-flight secondary ion mass spectrometry (ToF-SIMS) for showing that in the case of LNMO-based cathodes, a major part of the cathode impedance is related to the formation of a passivating interphase on the Al current collector. Remarkably, the impedance of this interphase can be mitigated by the targeted formation of a distinct passivating interphase, namely on the surface of the LNMO particles. The interplay between these interphases is discussed.

Introduction

The shift towards renewable and intermittent energy sources leads to a rising demand in affordable and benign energy storage solutions. Lithium-ion batteries (LIB) are the most prominent solution for mobile and stationary applications. Many efforts focus on increasing the gravimetric and volumetric energy density of LIB cells.[1] Significant advances have been achieved by deploying nickel manganese cobalt oxide (NMC) and lithium nickel cobalt aluminum oxides (NCA) on the cathode side and by addition of small amounts of silicon to the graphite anodes.[2,3] On the cathode side, the cobalt content has gradually been reduced, which is important with regard to cost reduction and environmental considerations.[4] Consequently, there is a strong incentive to eliminate cobalt completely from the cathode.[4,5] Lithium iron phosphate LiFePO$_4$ (LFP) is an obvious choice regarding price and safety. Consequently,

interest in LFP has resurged even for mobile applications. However, the energy density of LFP at the cell level is comparatively low (540 $\frac{Wh}{kg}$ compared to 690 $\frac{Wh}{kg}$ for LiNi$_{0.5}$Mn$_{1.5}$O$_4$ (LNMO) and 740 $\frac{Wh}{kg}$ for LiNi$_{0.8}$Mn$_{0.1}$Co$_{0.1}$O$_2$ (NMC811)).[6] Therefore, considerable efforts were made to improve the pack design with regard to the overall energy density.[7] LNMO is a promising candidate and has received considerable interest in recent years.[8–11] Its high reduction potential of 4.7 V vs. Li$^+$/Li compensates for the relatively low capacity (147 $\frac{mAh}{g}$ as compared to approx. 200 $\frac{mAh}{g}$ for NMC811).[12–14] However, LNMO cathodes suffer from accelerated degradation processes and high impedance, which need to be mitigated in order to achieve commercial viability.[15]

Different unfavorable side reactions in LNMO cathodes can increase the cell resistance. First, transition metal ions, predominantly Mn^{2+} ions, are dissolved in the liquid electrolyte and are then deposited on the anode, leading to graphite poisoning and fast capacity decay as well as impedance increase. Second, ethylene carbonate is oxidized on LNMO at potentials above 4.5 V vs. Li$^+$/Li.[16,17] In order to mitigate these side reactions, LNMO particles were coated with thin ion conducting layers, such as LiNbO$_3$.

An interesting topic in this field of research is also the interaction of electrolytes and electrode materials with the current collector. The salt LiPF$_6$ in the carbonate-based electrolyte is of particular importance, since it enables the usage of Al current collectors at potentials far above the dissolution potential of Al. This is due to the formation of a passivation layer, consisting of AlF$_3$ and Al$_2$O$_3$.[18,19] In the case of blank Al in contact to electrolytes, a passivating layer thickness of a few nanometers has been reported.[20–24] However, the passivation is not perfect, and various corrosion problems at the Al surface have been reported and linked to battery performance

[a] L. Pateras Pescara, A. Jaegermann, Dr. M. Cronau, Prof. Dr. B. Roling
Department of Chemistry and Center for Materials Science (WZMW)
University of Marburg
Hans-Meerwein-Strasse 4, 35032 Marburg (Germany)
E-mail: roling@staff.uni-marburg.de

[b] Dr. V. Mereacre, Dr. J. R. Binder
Karlsruhe Institute of Technology (KIT)
Institute for Applied Materials (IAM-ESS)
Hermann-von-Helmholtz-Platz 1, D-76344 Eggenstein-Leopoldshafen (Germany)

Batteries & Supercaps

Research Article
doi.org/10.1002/batt.202300352

**Chemistry
Europe**
European Chemical
Societies Publishing

deterioration.[25,26] Most prominently, pitting corrosion, Al dissolution and crevice corrosion have been discussed.[27] It has been shown that metallic impurities and the surface morphology of Al can influence the corrosion behavior in the cell.[28] Additionally, manufacturing defects from Al foil production or slurry coating can have an effect on the corrosion mechanisms at the Al surface, making the combined system of current collector, electrolyte and CAM rather complex.[23,29] Regarding LNMO, however, the interaction of the CAM with the electrolyte and the Al current collector does not seem to be of major interest in the recent literature.[16,26,30,31] As an exception, it has been reported that the impedance of LNMO electrodes is dominated by the resistance of an interphase between the active material particles and the Al current collector surface.[38] It was suggested that the interphase layer consists of AlF_3, however without characterizing the chemical composition of the layer.[38]

In this paper, we show that the interaction of CAM, electrolyte and current collector plays an important role for the impedance of LNMO cathodes. By combining electrochemical impedance spectroscopy (EIS) with focused ion beam/scanning electron microscopy (FIB/SEM) and time-of-flight secondary ion mass spectrometry (ToF-SIMS), we present evidence that the interphase formed on the current collector is indeed a fluoride-rich layer, the thickness and impedance of which is strongly influenced by the interphase on the CAM particles. Based on our experimental results, we propose means for mitigating the interphase impedance, which is essential for building high-power LNMO-based batteries.
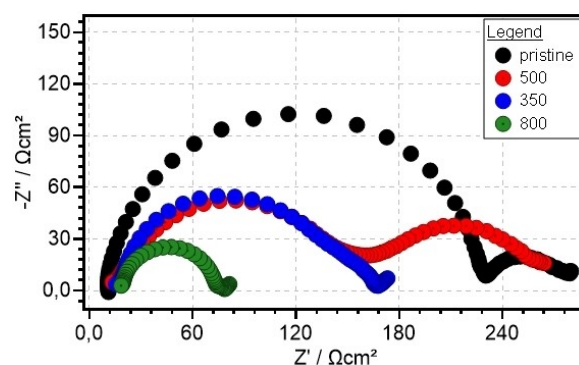
Results and Discussion

Figure 1 shows a galvanostatic charge/discharge cycle for LNMO composite electrode half cells at a rate of 0.1 C. In these half cells, the LNMO particles are either uncoated (pristine) or are coated by a $LiNbO_3$ layer, which has heat-treated at 350 °C, 500 °C, and 800 °C, respectively. Samples are labelled with
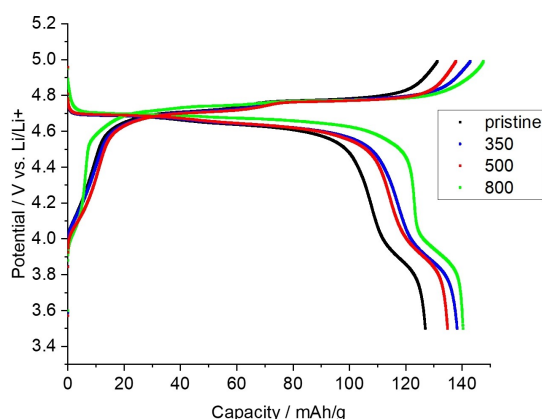
numbers reflecting the post-coating heat treatment temperature in degrees centigrade (e.g. sample 350), analogously to Mereacre et al.[32] As seen from Figure 1, the coating improves the discharge capacity, and the highest discharge capacity, which is close to the theoretical capacity of LNMO (147 mAh/g), is observed for the coated particles heat-treated at 800 °C. First-cycle Coulomb efficiencies were improved from 90 % for pristine LNMO to 92 % for the sample 350 and to 96 % for samples 500 and 800. The voltage profile of sample 800 lacks the distinct step in the charge profile at 4.75 V. This change in the voltage profile can be explained by a phase change from the ordered $P4_332$ phase to the disordered Fd-3 m phase, which is reported to take place above 700 °C.[30]

In order to elucidate the influence of the coating on the rate capability, impedance spectra were taken at a state of charge of 50 % (SOC50) in a frequency range from 100 kHz to 30 mHz, see Figure 2. The spectra are characterized by two semicircles and the onset of a Warburg impedance at low frequencies. The spectra were fitted by means of an equivalent circuit shown in Figure 3. The equivalent circuit is a Randles circuit with a $R_{IP} || C_{IP}$ element added in series, accounting for the impedance of interphases. The other elements of the circuit represent the separator resistance R_E, the charge transfer resistance R_{CT}, the double layer capacitance C_{DL}, and the Warburg impedance Z_W, which is related to Li diffusion in the LNMO particles. Although in the case of composite electrodes, transmission-line models are generally used for fitting impedance spectra,[33,34] we show in the SI that due to the low thickness, the high porosity of the LNMO electrode (~60 μm and 52 %, respectively) and the high ionic conductivity of the liquid electrolyte, the diameter of the low-frequency semicircle is, to a good approximation, determined by the charge transfer resistance R_{CT}. The capacitance of the high frequency semicircle
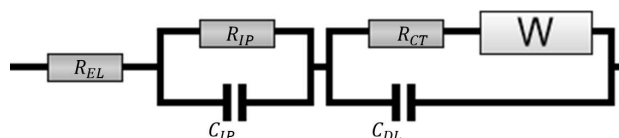

Figure 1. Galvanostatic charge/discharge curve of LNMO composite electrode half cells at a rate of 0.1 C. The LNMO particles are either uncoated (pristine) or coated by a $LiNbO_3$ layer, which is heat-treated at 350 °C, 500 °C, and 800 °C, respectively. The third cycle is shown and the discharge cycle is used for capacity determination.

Figure 2. Impedance spectra of LNMO electrodes at a state of charge of 50 % (SOC 50).

Figure 3. Equivalent circuit model used for fitting the impedance spectra in Figure 2.

Batteries & Supercaps

Research Article
doi.org/10.1002/batt.202300352

Chemistry Europe
European Chemical
Societies Publishing

is in the range of 1—2 μF/cm^2, see Table 1, which supports the assignment of this semicircle to the impedance of an interphase. In addition, the impedance spectrum of a LNMO cathode with high mass loading of approx. 40 mg/cm^2 shows that the high-frequency semicircle is not significantly influenced by the cathode thickness, see Figure SI2.

In the literature, a broad range of values for the interfacial impedance of LNMO cathodes has been reported, with values ranging from about 10 Ωcm.2 to about 300 Ωcm.2.[9,35] Often, values between 50 and 150 Ωcm.2 were found.[8,15,30,32,36,37] The origin of this broad range of values has not been clarified up to now. However, it has previously been reported that the impedance of LNMO electrodes is dominated by the resistance of an interphase between the active material particles and the Al current collector surface.[38] It was suggested that the interphase layer consists of AlF$_3$, however without characterizing the chemical composition of the layer.[38]

In order to obtain more information about the nature and thickness of the passivation layer on the Al current collector after cycling, the LNMO particles were dissolved from the current collector surface using N-methyl-2-pyrrolidone (NMP), and the Al surface was characterized by scanning electron microscopy with energy-dispersive X-ray spectroscopy (SEM/EDX) and by time-of-flight secondary ion mass spectrometry (ToF-SIMS). SEM micrographs of the Al surface shown in Figure 4 reveal a particulate interphase layer with particle size up to the micron range.

Low magnification images as seen in Figure 4 were taken to show representative sample areas. Higher magnification images and close ups of distinct features can be found in Figure 6, Figure SI1 and Figures SI5 and 6. Remarkably, the particles seem to be arranged along lines on the surface, which indicates that the surface corrosion takes place preferably at preexisting defects. As seen from the EDX line scan analysis of a single large particle in Figure 5 and from the SEM/EDX images in Figure 6, the particles are cone-shaped and are composed of Al and F. The higher atomic fraction of F as compared to Al in the center of the particle together with the expectation that bulk Al below
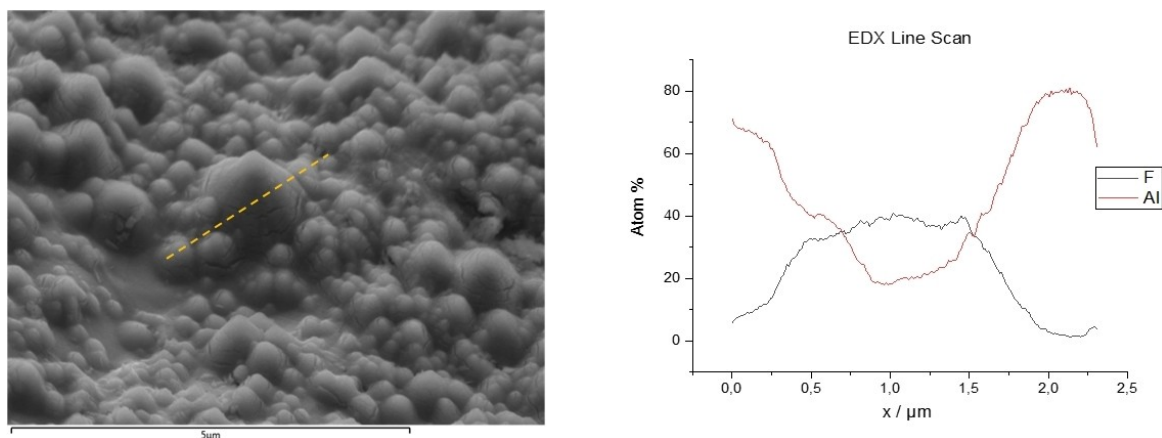
Table 1. Discharge capacities and equivalent-circuit fitting results for the impedance of the LNMO electrodes.

| LNMO Sample	$C_{discharge}$ [$\frac{mAh}{g}$]	R_{IP} [Ωcm^2]	C_{IP} [$\frac{F}{cm.2}$]	R_{CT} [Ωcm^2]	C_{DL} [$\frac{F}{cm^2}$]
pristine	127	2.0×10^2	1.2×10^{-6}	4.4×10^1	4.0×10^{-3}
350	138	9.8×10^1	1.6×10^{-6}	4.3×10^1	4.2×10^{-4}
500	133	1.2×10^2	1.4×10^{-6}	9.6×10^1	8.9×10^{-4}
800	141	5.1×10^1	1.2×10^{-6}	5.5×10^0	5.7×10^{-3}
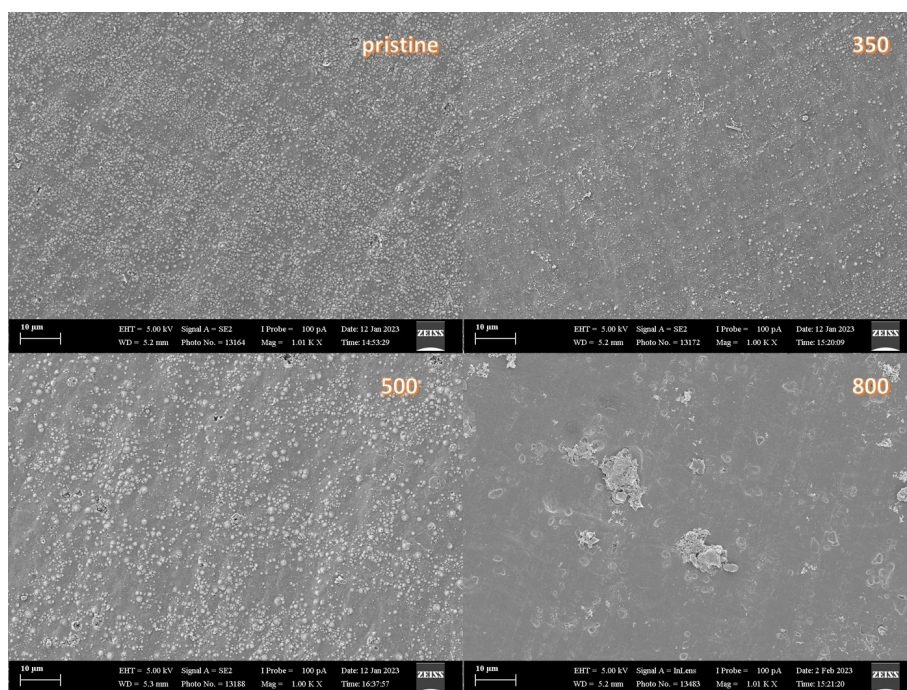
Figure 4. SEM images of the Al current collector surface after cycling the LNMO cathodes and dissolving the LNMO particles. The surface is covered by sub-micron and micron-sized particles. In the case of LNMO particles coated with a LiNbO$_3$ layer heated-treated at 800 °C (sample 800), virtually no particles are found on the surface. Instead, residues of active material particles are found, indicating that the active material particles are bound more strongly to a current collector with less fluoride-rich layer, most likely AlF$_3$. Furthermore, it was observed that the separation process upon immersion in NMP took much longer for the sample 800 compared to the other samples.

Batteries & Supercaps

Research Article
doi.org/10.1002/batt.202300352

Chemistry Europe
European Chemical
Societies Publishing

Figure 5. SEM image and EDX line scan of the Al current collector surface after cycling of the LNMO cathode. The dashed line in the SEM image indicates the EDX line scan across a large particle with Al and F EDX signals, indicating that the particle consists of AlF_3.
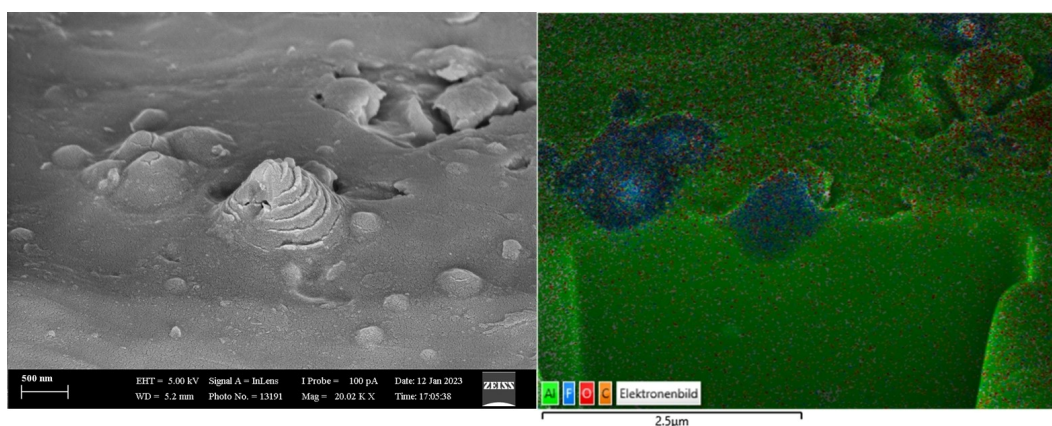

Figure 6. Left) SEM image of a fluoride-rich particle. Right) FIB cut of a particle found on the current collector of the cathode with $LiNbO_3$-coated particles heat-treated at 500 °C. The particles are cone-shaped and tend to develop concentric cracks, resulting in a cabbage-like appearance. This indicates a pitting corrosion mechanism involved in the particle growth.[26] Areas that are not overgrown with fluoride-rich particles show an oxygen EDX signal, most likely due to a native Al_2O_3 passivation layer.

the particles contributes also to the Al EDX signal gives indication that the particles consist of AlF_3.

A FIB cut into the current collector reveals that the fluoride-rich layer is deposited on the Al surface with little penetration into the bulk. At particle-free positions of the Al surface, a thin Al_2O_3 layer seems to exist. Results from time-of-flight secondary ion mass spectrometry (ToF-SIMS) support these findings, see Figure 7.
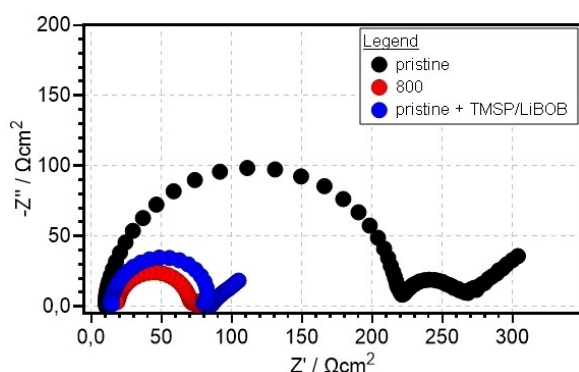
In order to estimate the overall coverage of the Al current collectors by AlF_3 in the different cathodes, we recorded the maximum fluorine EDX signal in surface areas of the current collectors, which were densely covered by large particles, most likely AlF_3 (Figure SI1), and normalized all fluorine EDX signals by this maximum signal. In Figure 8, we plot the interphase resistance R_{IP} obtained from fits of the impedance spectra versus the normalized fluorine EDX signal. The strong increase of the interphase resistance R_{IP} with the normalized fluorine EDX signal gives strong indication that the fluoride-rich passivation layer is responsible for the high interphase resistance. Apparently, the $LiNbO_3$ coating of the LNMO particles
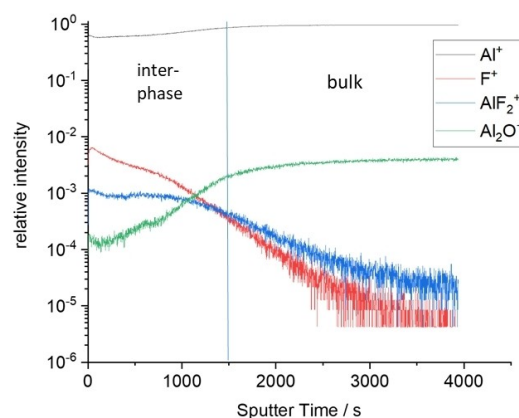
Figure 7. TOF-SIMS depth profiles of the Al current collector surface after cycling and dissolution of the pristine LNMO particles. High values of the Al_2O^+, generated by incorporation of oxygen from the sputter beam, indicate bulk Al. The fragment AlF_2^+ indicates an AlF_3 interphase layer. The vertical blue line is added as a guide to the eye for indicating the transition from the interphase to bulk Al.
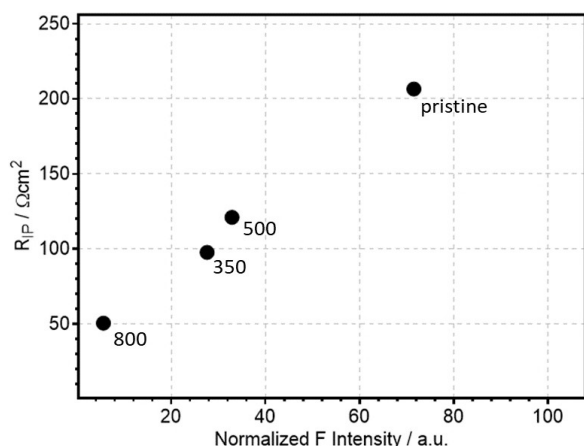
Figure 8. Interphase resistance of the LNMO cathode R_{IP} plotted versus the normalized intensity of the fluorine EDX signal obtained on the Al current collector surface. Values are obtained by integrating the F EDX peaks. For corresponding EDX spectra see Figure SI4.

Figure 9. Impedance spectra of LNMO composite cathodes with uncoated LNMO particles in two different electrolytes: additive-free electrolyte and electrolyte with 1 wt% TMSP and LiBOB as additives. The TMSP/LiBOB additive reduces the interphase resistance to values similar to cathodes with LiNbO$_3$-caoted LNMO particles heat-treated at 800°C.

case of excessive HF is unclear at present. The SEM images in Figures SI5 and SI6 indicate that preexisting defects in the Al surface play a role. However, the exact growth mechanism of the fluoride-rich interphase needs further investigation in the future. In the case of NMC and NCA with lower operation voltages, excessive amounts of HF and high-resistance interphases do not form.

In the case of LNMO, the oxidation reaction can be inhibited by a LiNbO$_3$ coating of LNMO particles. This coating acts as an artificial cathode-electrolyte interphase (CEI). Heat treatment of the LiNbO$_3$ coating at 800°C seems to mitigate ethylene carbonate oxidation most effectively. Thus, the reduced cathode impedance after LiNbO$_3$ coating is not caused by the CEI impedance itself, as reported previously,[9,32,37,40] but by the suppression of ethylene carbonate oxidation and of fluoride-rich interlayer formation on the Al current collector by the coating.

This finding implicates alternative strategies to reduce the LNMO cathode impedance, namely the usage of electrolyte additives for CEI formation. An electrolyte containing an HF scavenger (e.g., tris(trimethylsilyl)phosphite, TMSP) and a corrosion inhibitor (e.g., lithium bis(oxalato)borate, LiBOB) should also be capable of mitigating the interphase impedance on the Al current collector. LiBOB has been shown to improve the capacity retention of LNMO electrodes by forming a CEI consisting of cross-linked borates and polycarbonates.[40] TMSP is known to scavenge HF from the electrolyte, preventing subsequent degradation processes. Furthermore, TMSP-based CEIs reduce electrolyte decomposition reactions at high voltage.[41] We added 1 wt% TMSP and 1 wt% LiBOB to the carbonate-based electrolyte and carried out electrochemical characterization with pristine LNMO. As shown in Figure 9, the interphase impedance measured at SOC50 exhibits values similar to that after LiNbO$_3$ coating and heat treatment at 800°C.

Conclusions

The combination of electrochemical impedance spectroscopy, FIB/SEM/EDX and ToF-SIMS gives strong indication that a fluoride-rich passivation layer, most likely an AlF$_3$ layer, on the surface of the Al current collector contributes strongly to the impedance of LNMO cathodes and thus limits the rate capability of such cathodes. The origin of this passivation layer is related to the oxidation of ethylene carbonate at the LNMO particle surface at potential above 4.5 V, which leads to the formation of water, and in turn, to PF$_6^-$ anion hydrolysis, HF and AlF$_3$ formation. The ethylene carbonate oxidation can be mitigated by the formation of a cathode/electrolyte interphase (CEI) on the LNMO particles, e.g. by coating the LNMO particles with a LiNbO$_3$ interphase or by adding CEI-forming additives, such as LiBOB, and HF scavenging additives, such as TMSP.

mitigates the formation of passivation layer as demonstrated in Figure 4 and reduces the interphase resistance.

In general, AlF$_3$ formation on Al current collectors takes place by HF attack. HF can be formed via hydrolysis of PF$_6^-$ anions by traces of water in the electrolyte. However, as described by Kühn et al.,[39] HF can also be generated via the chemical oxidation of ethylene carbonate, see Figure SI3. This oxidation reaction produces water, which leads to further hydrolysis of PF$_6^-$ anions and to HF formation. The reaction takes place on the surface of uncoated LNMO particles at potentials above 4.5 V vs. Li$^+$/Li and is thus a distinct drawback of LNMO cathodes and other high-voltage cathode materials. The reaction produces excessive HF and leads to the formation of a thick fluoride-rich interlayer, most likely AlF$_3$, on the Al current collector and, in turn, to a high interfacial impedance. Thus, a thick fluoride-rich interlayer should be avoided, while a thin layer with a thickness in the nm range is of upmost importance for the passivation of the Al current collector. The reason for the strong growth of the fluoride-rich layer in the

Batteries & Supercaps

Research Article
doi.org/10.1002/batt.202300352

Chemistry Europe
European Chemical
Societies Publishing

Experimental Section

Electrode preparation

Single crystalline LNMO was purchased from MSE supplies (Tucson, USA). The material was either used pristine or coated with a LiNbO$_3$ layer by a H$_2$O$_2$-activated procedure as described elsewhere.[32] Prior to slurry casting, the LNMO particles were heat-treated at either 350, 500 or 800 °C for 1 h under O$_2$ atmosphere. LNMO composite electrodes were prepared from a N-Methyl-2-pyrrolidone-based (NMP 99.5%, Alfa Aesar, Thermo Fischer GmbH, Kandel, Germany) slurry with 80 wt% LNMO (97.0%, MSE Supplies), 10 wt% C-NERGY SUPER C65 carbon black (Timcal, Bodio, Switzerland) as conductivity additive, and 10 wt% polyvinylidene fluoride (PVDF, Solvay GmbH, Hannover). First, the binder was dissolved in NMP at 65 °C. LNMO and carbon black powders were added in 10 small portions and mixed by means of a T 25 disperser (IKA, Staufen, Germany). The resulting slurry was cast onto an aluminum foil (Rotilabo 30 μm, Roth, Karlsruhe, Germnay). The thickness of the films was adjusted using a ZAA 2300 automatic film applicator (Zehntner, Sissach, Switzerland). The foils were dried for 24 hours at 70 °C under air atmosphere and transferred into an argon filled glovebox (Unilab, MBraun, Germany, $X_{H2O} < 1$ ppm, $X_{O2} < 1$ ppm). Subsequently, the films were calendered using a hot rolling press (MSK-HRP-01, MTI Corporation, Richmond, USA), starting at an air gap of 200 μm and successively reducing the air gap down to 60 μm in steps of 10 μm. During the calendering process, the thickness and porosity of the electrolyte were reduced from 200 μm and 85% to 60 μm and 52%. Electrode coins with a diameter of 11.75 mm were punched out of the electrode films and dried in vacuum until a pressure of 5×10^{-6} mbar was reached. Prior to cell assembly, the weight of the coins was determined using a laboratory scale (Kern ALJ, Kern & Sohn GmbH, Balingen-Frommern, Germany).

Cell assembly

Half cells in 3-electrode configuration were assembled using TSC Battery containments (rhd Instruments, Darmstadt, Germany). Lithium foil was used as counter and reference electrode. Two layers of Whatman fiber glass separators and one additional layer of Celgard-3000 separator were employed, and a mixture of ethylene carbonate and ethyl methyl carbonate containing 1 M LiPF$_6$ was used as electrolyte (Pureelyte, Sigma Aldrich). The stack pressure was controlled by means of a compression spring and adjusted by counting the revolutions of the compression screw. With a displacement of 4 mm and a spring constant of 2.4 N/mm, a stack pressure of 0.085 MPa was reached. All cell assembly steps were carried out inside an argon filled glovebox (Unilab, MBraun, Germany, $X_{H2O} < 1$ ppm, $X_{O2} < 1$ ppm). The water content of the electrolyte was checked by Karl Fischer titration to be below 10 ppm at all times. After sealing, the cells rested for at least 12 h and were subsequently subjected to the cycling procedures and the impedance measurements.

Galvanostatic cycling

Galvanostatic cycling was carried out in a two-electrode setup (TSC battery cell, rhd instruments, Darmstadt, Germany) with the composite cathode acting as working electrode and with metallic lithium acting as counter electrode. Cycling at 0.1 C was carried out at 25 °C between 3.5 V and 5.0 V as lower and upper cutoff potential, respectively, using a Maccor battery cycler (MACCOR Inc., Tulsa, USA). Discharge capacities were determined from the third discharge cycle at 0.1 C.

Electrochemical impedance spectroscopy

The electrochemical impedance measurements were carried out by means of a Multi Autolab/M101 equipped with an FRA32 M impedance module (Metrohm Autolab BV, Utrecht, Netherlands) at 50% state of charge (SOC50). After leveling to SOC50, the cells rested at OCP for 24 h before starting the EIS measurements. An AC voltage amplitude of 10 mV was applied and the frequency range extended from 10^5 Hz to 3×10^{-2} Hz. All impedance data was acquired in a 3-electrode configuration with a Li metal reference electrode. RelaxIS3 was employed for impedance analysis (rhd instruments, Darmstadt, Germany).

FIB-SEM/EDX analysis

The cycled cells were disassembled inside an argon filled glovebox, and the cathode was recovered. In order to remove the LNMO particles from the Al current collector, the cathodes were immersed in N-methyl-2-pyrrolidone (NMP). The current collector was then rinsed with 1 mL NMP and 1 mL of dimethyl carbonate (DMC) in order to remove both residual PVDF and conductive salt. The current collector was attached to a SEM sample holder with conductive carbon glue. The final sample was dried in vacuum (5×10^{-6} mbar), sputtered with gold and transferred to the FIB-SEM device in an argon filled transfer chamber. FIB milling, SEM and EDX measurements were performed using a Zeiss Crossbeam 550 Gemini 2 (Zeiss, Jena, Germany) device equipped with a UltimMax EDX detector (Oxford Instruments, Abingdon, UK). All EDX data was recorded with a current of 100 pA for 30 minutes at 1000x magnification.

ToF-SIMS analysis

Samples for ToF-SIMS analysis were pretreated analogously to the SEM samples. ToF-SIMS analysis was performed on an ION-TOF 4 (ION-TOF GmbH, Münster, Germany) in the interlaced mode, using O$_2^+$ as sputter beam (120 nA) and Bi$^+$ as primary beam (1 pA). The electron flood gun was used for charge compensation. A window of 300×300 μm^2 was used for sputtering and the analysis window was set to 100×100 μm^2.

Conflict of Interests

The authors declare no conflict of interest.

Data Availability Statement

The data that support the findings of this study are available from the corresponding author upon reasonable request.

Batteries & Supercaps

Research Article
doi.org/10.1002/batt.202300352

Chemistry Europe
European Chemical
Societies Publishing

[1] J. U. Choi, N. Voronina, Y. Sun, S. Myung, *Adv. Energy Mater.* **2020**, *10*, 2002027.

[2] A. Manthiram, *Nat. Commun.* **2020**, *11*, 1550.

[3] X. Zuo, J. Zhu, P. Müller-Buschbaum, Y.-J. Cheng, *Nano Energy* **2017**, *31*, 113–143.

[4] D. Darbar, T. Malkowski, E. C. Self, I. Bhattacharya, M. V. V. Reddy, J. Nanda, *Mater. Today Energy* **2022**, *30*, 101173.

[5] H. Zhao, W. A. Lam, L. Sheng, L. Wang, P. Bai, Y. Yang, D. Ren, H. Xu, X. He, *Adv. Energy Mater.* **2022**, *12*, 2103894.

[6] G. Xu, X. Liu, A. Daali, R. Amine, Z. Chen, K. Amine, *Adv. Funct. Mater.* **2020**, *30*, 2004748.

[7] Reuters, *Automot. News Eur.* **2023**.

[8] P. Axmann, G. Gabrielli, M. Wohlfahrt-Mehrens, *J. Power Sources* **2016**, *301*, 151–159.

[9] H. Duncan, Y. Abu-Lebdeh, I. J. Davidson, *J. Electrochem. Soc.* **2010**, *157*, A528–A535.

[10] J. Chong, S. Xun, J. Zhang, X. Song, H. Xie, V. Battaglia, R. Wang, *Chem. Eur. J.* **2014**, *20*, 7479–7485.

[11] K. Kanamura, W. Hoshikawa, T. Umegaki, *J. Electrochem. Soc.* **2002**, *149*, A339.

[12] R. Jung, M. Metzger, F. Maglia, C. Stinner, H. A. Gasteiger, *J. Electrochem. Soc.* **2017**, *164*, A1361–A1377.

[13] F. Xin, H. Zhou, X. Chen, M. Zuba, N. Chernova, G. Zhou, M. S. Whittingham, *ACS Appl. Mater. Interfaces* **2019**, *11*, 34889–34894.

[14] Y. Fan, J. Wang, X. Ye, J. Zhang, *Mater. Chem. Phys.* **2007**, *103*, 19–23.

[15] J. W. Kim, D. H. Kim, D. Y. Oh, H. Lee, J. H. Kim, J. H. Lee, Y. S. Jung, *J. Power Sources* **2015**, *274*, 1254–1262.

[16] G. Liang, V. K. Peterson, K. W. See, Z. Guo, W. K. Pang, *J. Mater. Chem. A* **2020**, *8*, 15373–15398.

[17] J. F. Browning, L. Baggetto, K. L. Jungjohann, Y. Wang, W. E. Tenhaeff, J. K. Keum, D. L. Wood, G. M. Veith, *ACS Appl. Mater. Interfaces* **2014**, *6*, 18569–18576.

[18] X. Zhang, T. M. Devine, *J. Electrochem. Soc.* **2006**, *153*, B344.

[19] M. Morita, T. Shibata, N. Yoshimoto, M. Ishikawa, *Electrochim. Acta* **2002**, *47*, 2787–2793.

[20] A. Gabryelczyk, S. Ivanov, A. Bund, G. Lota, *J. Energy Storage* **2021**, *43*, 103226.

[21] S. Song, T. Richardson, G. Zhuang, T. Devine, J. Evans, *Electrochim. Acta* **2004**, *49*, 1483–1490.

[22] X. Wang, E. Yasukawa, S. Mori, *Electrochim. Acta* **2000**, *45*, 2677–2684.

[23] X. Zhang, B. Winget, M. Doeff, J. W. Evans, T. M. Devine, *J. Electrochem. Soc.* **2005**, *152*, B448.

[24] S. S. Zhang, T. R. Jow, *J. Power Sources* **2002**, *109*, 458–464.

[25] T. C. Hyams, J. Go, T. M. Devine, *J. Electrochem. Soc.* **2007**, *154*, C390.

[26] L. Guo, D. B. Thornton, M. A. Koronfel, I. E. L. Stephens, M. P. Ryan, *J. Phys. Energy* **2021**, *3*, 032015.

[27] S.-T. Myung, Y. Hitoshi, Y.-K. Sun, *J. Mater. Chem.* **2011**, *21*, 9891.

[28] J. W. Braithwaite, A. Gonzales, G. Nagasubramanian, S. J. Lucero, D. E. Peebles, J. A. Ohlhausen, W. R. Cieslak, *J. Electrochem. Soc.* **1999**, *146*, 448–456.

[29] X. Zhang, P. N. Ross, R. Kostecki, F. Kong, S. Sloop, J. B. Kerr, K. Striebel, E. J. Cairns, F. McLarnon, *J. Electrochem. Soc.* **2001**, *148*, A463.

[30] T.-F. Yi, J. Mei, J.-R. Zhu, *J. Power Sources* **2016**, *316*, 85–105.

[31] P. Zhu, D. Gastol, J. Marshall, R. Sommerville, V. Goodship, E. Kendrick, *J. Power Sources* **2021**, *485*, 229321.

[32] V. Mereacre, P. Stüble, A. Ghamlouche, J. R. Binder, *Nanomaterials* **2021**, *11*, 548.

[33] M. Cronau, M. Kroll, M. Szabo, F. Sälzer, B. Roling, *Batteries & Supercaps* **2020**, *3*, 611–618.

[34] M. Cronau, A. Paulus, L. P. Pescara, M. Kroll, D. Renz, J. A. Mekontso, A. Marx, B. Roling, *Batteries & Supercaps* **2022**, *5*, e202200194.

[35] G. Gabrielli, P. Axmann, T. Diemant, R. J. Behm, M. Wohlfahrt-Mehrens, *ChemSusChem* **2016**, *9*, 1670–1679.

[36] J. Li, Y. Zhang, J. Li, L. Wang, X. He, J. Gao, *Ionics* **2011**, *17*, 671–675.

[37] H. Kim, D. Byun, W. Chang, H.-G. Jung, W. Choi, *J. Mater. Chem. A* **2017**, *5*, 25077–25089.

[38] D. Pritzl, A. E. Bumberger, M. Wetjen, J. Landesfeind, S. Solchenbach, H. A. Gasteiger, *J. Electrochem. Soc.* **2019**, *166*, A582–A590.

[39] S. P. Kühn, K. Edström, M. Winter, I. Cekic-Laskovic, *Adv. Mater. Interfaces* **2022**, *9*, 2102078.

[40] Y. Dong, B. T. Young, Y. Zhang, T. Yoon, D. R. Heskett, Y. Hu, B. L. Lucht, *ACS Appl. Mater. Interfaces* **2017**, *9*, 20467–20475.

[41] H. Wang, S. Chen, Y. Li, Y. Liu, Q. Jing, X. Liu, Z. Liu, X. Zhang, *Adv. Energy Mater.* **2021**, *11*, 2101057.